

Tutorial: the seismic response to strong vertical velocity change

Ian F. Jones^{1*}

Abstract

Conventional seismic data processing, whether pre-stack data conditioning or migration, is designed with the theory of P-wave reflected energy in mind for travel paths involving only a single reflection. Hence, any energy propagating with other modes or travel paths is not dealt with appropriately during conventional processing. It is primarily for this reason that we spend so much time pre-conditioning seismic data to meet the assumptions of the subsequent processes such as migration. Here I consider a typical North Sea environment where there are both strong vertical compaction gradients and high velocity contrasts in the layered Chalk Formation. I assess the behaviour of refracted and mode-converted seismic arrivals when subjected to conventional processing in order to explain how they give rise to anomalous events that contaminate migrated common reflection point gathers and images.

Introduction

Although the title of this article is somewhat generic, this study originated in a Chalk imaging project, using marine streamer data from the North Sea, where the overburden has a very strong vertical velocity gradient in places, due to compaction, and the Chalk itself comprises several layers with high velocity contrast. Data acquired in a surface streamer survey, where there is significant S-to-P mode conversion of the upcoming wavefield at the seabed, may contain refracted and mode-converted seismic arrivals, such as those starting as P waves, converting to S, reflecting as S, and then converting back to P (denoted as PSSP), as well as other conversion paths (e.g., PSPP or PPSP). In shallow water, as was the case in this study, significant mode-converted energy is recorded even at modest source-receiver offsets. Ideally, data pre-conditioning steps, such as linear noise removal, should remove these events prior to velocity estimation and migration. In practice, spurious remnants of them often remain, and are then dealt with as if they were P-wave reflection energy, giving rise to anomalous behaviour in the migrated data.

Here I present a modelling study to assess the behaviour of Chalk-related seismic reflection and refraction events. Diving rays and refractions in the overburden resulting from large vertical compaction velocity gradients are also addressed, as remnant energy from these events impinges on the underlying Chalk reflections. I attempt to highlight some of this behaviour qualitatively, to give insight into observed effects on real data during velocity model building and in images after migration.

Modelling study

The P-wave velocities used in the forward modelling were based on a high-resolution tomographic pre-stack depth migration (preSDM) model derived in a commercial preSDM project over a region in the North Sea with water depths of about 80 m and the top Chalk horizon at about 1 km depth. The tomography cell size used in the region of the Chalk was 50 m × 50 m × 50 m, in order to resolve thin intra-Chalk layering. The velocity model was verified and calibrated using available well sonic logs. Density was estimated using a modified Gardner relationship, calibrated to the available density logs and assuming reasonable values in the shallow section, which was not logged. In addition, some literature was reviewed to determine a range of realistic S-wave velocity and density values near the seabed (e.g., Carbone et al., 1998; Muyzert, 2006; Shillington et al., 2008).

Modelling was performed using both 2D finite difference (FD) and ray-tracing techniques, both acoustically and elastically. Modelling was conducted using both the Landmark ProMax package, which can perform isotropic acoustic FD modelling using gridded models, and with ION GXT's GXII 2D modelling code, which can perform anisotropic visco-elastic or visco-acoustic ray-tracing or FD modelling with layered models. All modelling in this study was isotropic, and for investigation of post-critical phase change, attenuation was turned off to avoid further change in the wavelet's phase. The FD forward modelling employed a grid size small enough to avoid numerical dispersion in the FD propagation. The maximum source-receiver offset was

¹ ION-GXT Imaging Solutions, 1st Floor, Integra House, Vicarage Road, Egham, Surrey TW20 9JZ, UK.

* Corresponding author, E-mail: Ian.Jones@iongeo.com

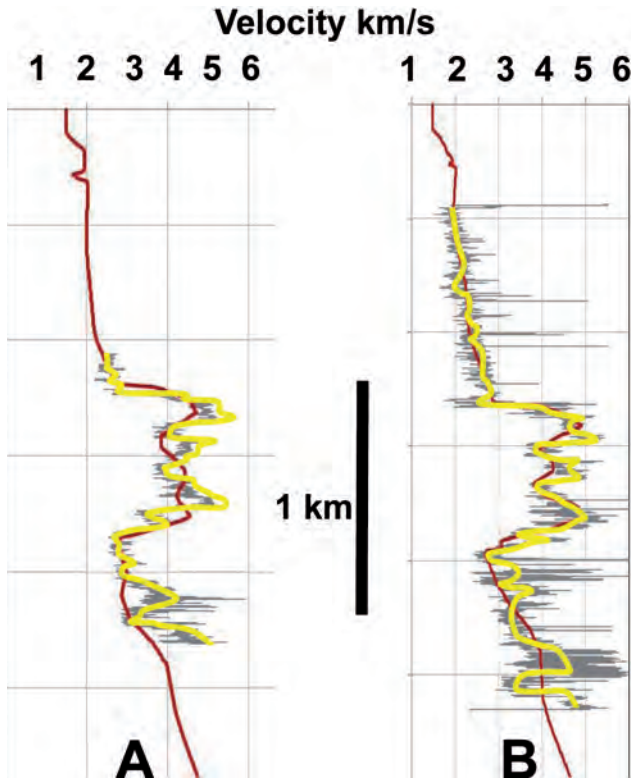


Figure 1 Velocity logs and their smoothed versions (yellow lines). The red lines are from an intermediate tomographic model.

5 km, the depth of the model was 5 km, and the modelled record lengths were 3 s.

Three different models were used, with differing levels of complexity, to emphasize various aspects of the issues under investigation:

- Model 1: was a gridded model with significant lateral and vertical velocity variation, as used in the commercial production preSDM project. A zero-phase Ricker wavelet with a peak frequency of 30 Hz was used in the FD modelling, which was purely acoustic. The objective of creating synthetic data using this model was to reproduce the overall gross features observed in the real data.
- Model 2 was a 1D velocity model resembling the vertical velocity profile at one of the well locations where we had detailed density and velocity information. Interval velocity compaction gradients were included with the form $V(z) = V(0) + kz$, where z is the depth in metres below sea surface and k is the compaction coefficient in units of s^{-1} . A zero-phase Ricker wavelet with a peak frequency of 18 Hz was used in the FD modelling, which was performed both acoustically and elastically. The objective of creating data with this model was to prevent any structural bias affecting the conclusions because local structural dip would affect the direction of critically incident raypaths at interfaces.
- Model 3 was a simple half-space, with no water layer, representing the sediment–Chalk interface to highlight

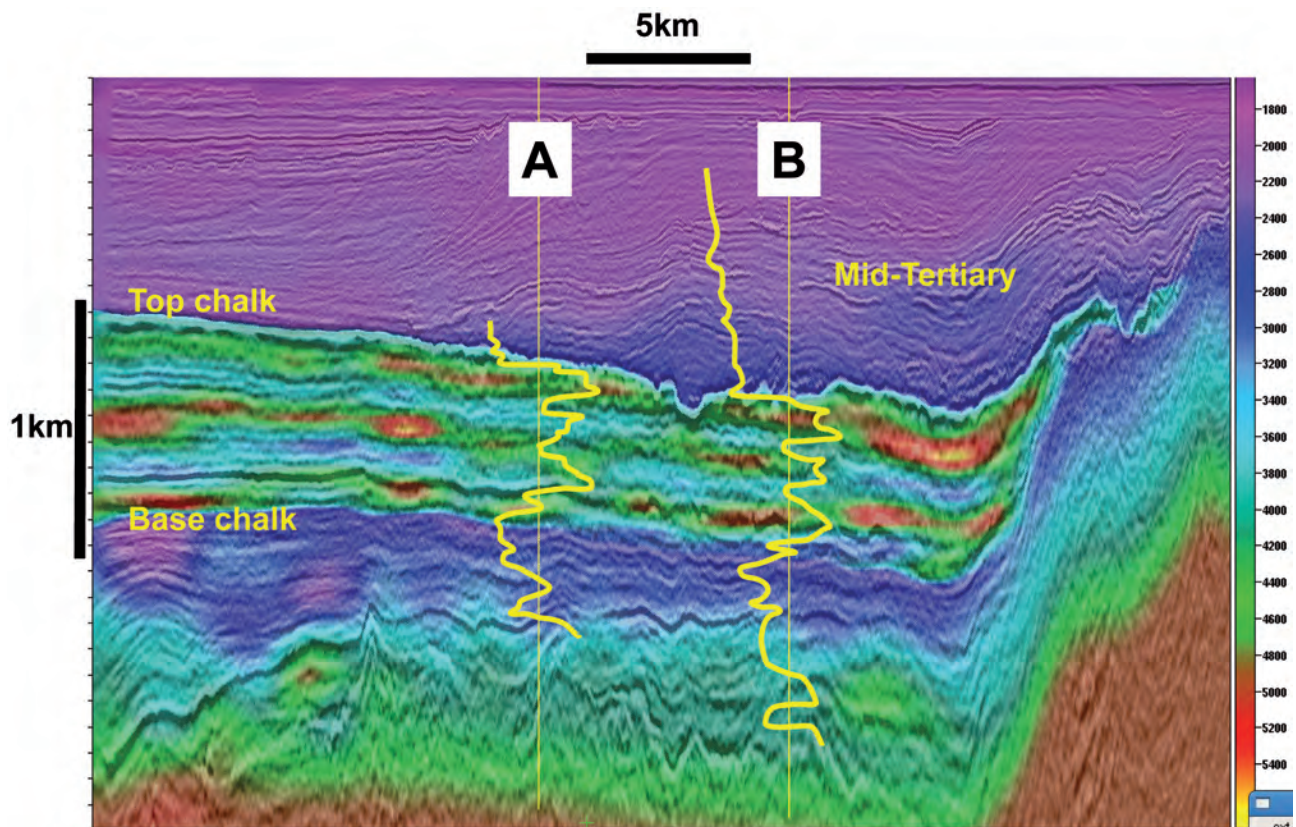


Figure 2 Smoothed velocity logs superimposed on the real data preSDM image, with tomographic interval velocity colour overlay (Model 1). The wells are from nearby locations, so do not tie the line perfectly.

the mode-conversion effects and also the phenomenon of Kirchhoff and NMO travel-time bifurcation. Modelling was purely acoustic with an upper layer velocity of 2700 m s⁻¹ and a lower velocity of 4800 m s⁻¹, these values being representative of the real velocities observed in the sediment and Chalk, respectively.

For the initial tests, an absorbing surface boundary condition was used in the FD modelling, but later, for assessment of surface-related multiples, the surface boundary condition was set to be reflecting. Unless otherwise stated, the real data were band-limited to make them better resemble the modelled data in all comparisons.

The study concentrated on a single representative in-line and four nearby wells, two of which (A and B) are shown in Figure 1. A depth-migrated seismic section with these wells superimposed shows at least three high-velocity bands within the Chalk and a strong compaction gradient above it (Figure 2). The background interval velocity superimposed on Figure 2 shows the high-resolution tomographic model from the commercial preSDM project (Model 1). The simplified 1D layered model used for the detailed analysis is shown in Figure 3 (Model 2), but it is really only the mid-Tertiary and top Chalk events that concern us, because those horizons generate the mode-converted and other events of interest here.

Observations from acoustic modelling

Many of the ‘non-flat’ events seen in CRP gathers at the mid-Tertiary and top Chalk levels are associated with post-critical reflection energy, which is prevalent here due to the very strong velocity contrasts at those layers. These events are exacerbated by the significant vertical compaction in part of the area, for example near well B in Figure 2: ignoring the mid-Tertiary boundary, the velocity increases from about 1550 m s⁻¹ at 150 m depth just below the seabed to about 2550 m s⁻¹ at about 1100 m depth. Although at the well location the vertical compaction gradient is ~1.0 s⁻¹, in the simplified 1D isotropic models I used a more modest value of ~0.2 s⁻¹, representative of other parts of the region. The seabed reflection also becomes post-critical for short offsets due to the shallow water:

- the critical angle at the seabed is about 70°, which corresponds to an offset less than 700 m;
- the critical angle at mid-Tertiary is about 40°, which corresponds to an offset less than 1400 m, hence most of the higher-order moveout events seen for this event are post-critical; and
- the critical angle at top Chalk is about 30°, which corresponds to an offset less than 1000 m, hence most of the far-offset events at top Chalk level are post-critical.

Figures 4–6 show a selection of gathers along the modelled line, created with acoustic modelling using Model 1, as shown in the colour overlay in Figure 2. This is the most complex model used, with significant structural variation, and was the model used in the commercial preSDM project. The CMP

gathers of the raw modelled data are shown in Figure 4, after NMO using the corresponding RMS velocity in Figure 5, and after preSDM using the correct model, i.e., that used to create the synthetic data, in Figure 6. Real 3D preSDM data from an intermediate stage in the production project (i.e., not the final gathers) are shown in Figure 7: these gathers exhibit many of the features seen in the modelled data.

For the real data from the commercial project, which were migrated anisotropically, the reflection component of these events should still be flat on the common reflection point (CRP) gathers beyond the critical angle. At large angles of incidence the moveout is very sensitive to anisotropic parameter error, so in the velocity model building, the angle gathers used were muted to about 50°; hence the higher angles shown in the CRP gathers here were not constrained to be flat.

Simplified modelling to help understand complex arrivals

The moveout behaviour observed in the FD modelling performed with the complex velocity model does indeed resemble the behaviour in the observed data. However, to better understand the nature of the observed events, I start the analysis by considering some grossly simplified models, using both FD and ray-tracing methods, and then move on to introducing converted modes in the modelling by using elastic modelling instead of acoustic modelling.

FD modelling produces all families of events simultaneously, so to better understand where the refraction and converted modes originate, I have done more specific ray-trace modelling for isolated selected events. In addition to the converted modes reflecting at the mid-Tertiary and the top Chalk, there are other non-reflected events, such as the diving rays, water bottom refractions, and mid-Tertiary post-critical events, all of which misbehave when treated as if they were P-wave reflection arrivals. Also, in addition to the real events that are not P-wave reflections, we also have some travel-time bifurcation artefacts, produced during NMO or Kirchhoff migration, that need to be considered.

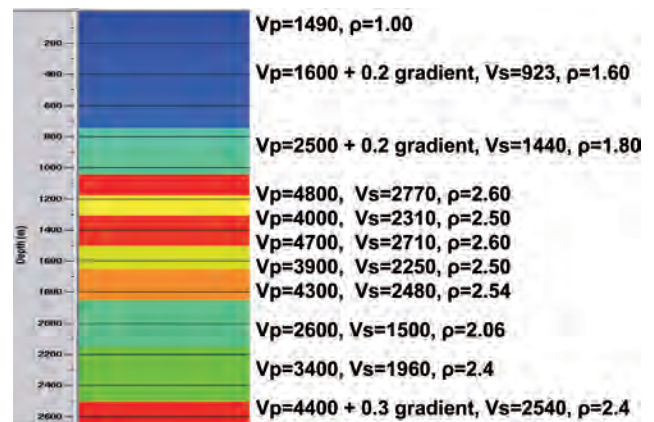


Figure 3 Model 2, used for 1D acoustic and elastic modelling, based on velocity profile near well A.

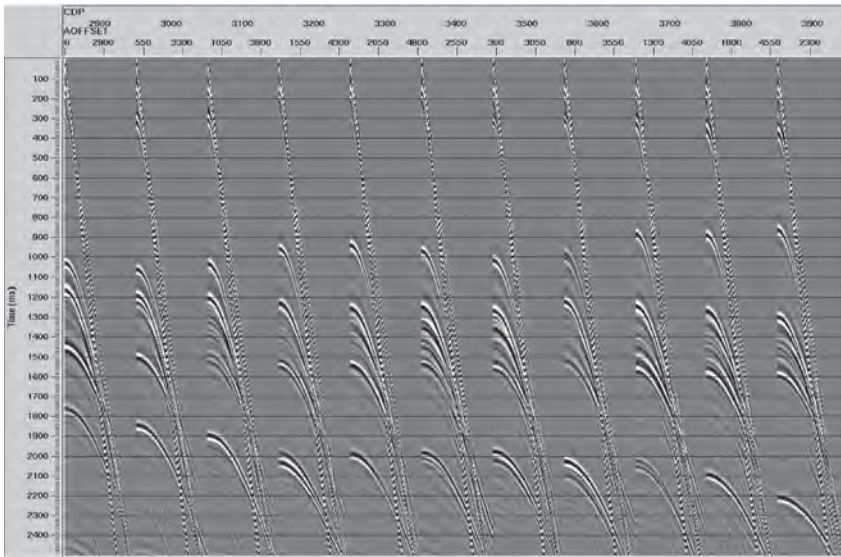


Figure 4 CMP gathers for the FD isotropic acoustically modelled data: 30 Hz peak frequency wavelet, maximum offset 5 km, without surface-related multiples, corresponding to the interval velocity model shown in Figure 2 (Model 1).

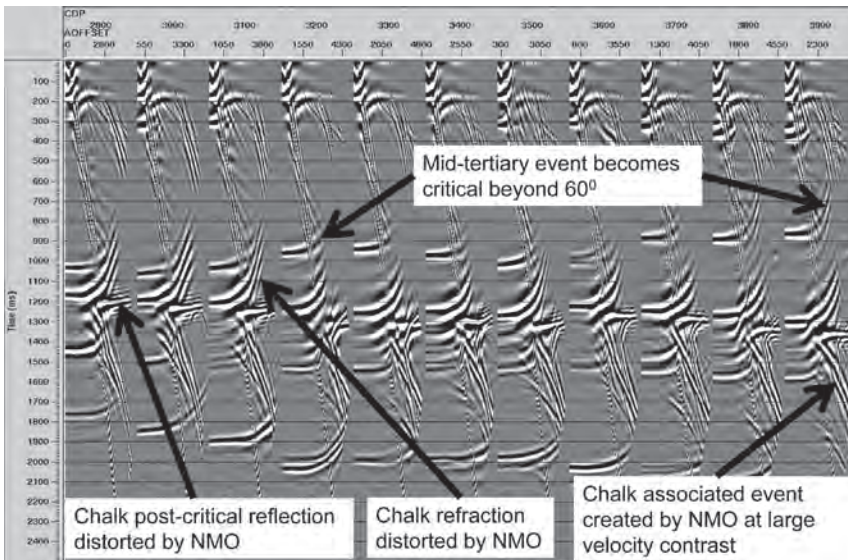


Figure 5 CMP gathers from Figure 4 after NMO correction. Already we see various anomalous events: for the mid-Tertiary event around 1000 ms there is apparent higher order moveout, which is in part post-critical refracted energy, and also higher order moveout from ray bending, both at interfaces and due to vertical compaction gradients. At the Chalk reflector, at about 1200 ms, there are linear upward and downward trending events. These are refracted events from the top Chalk being distorted by the NMO correction.

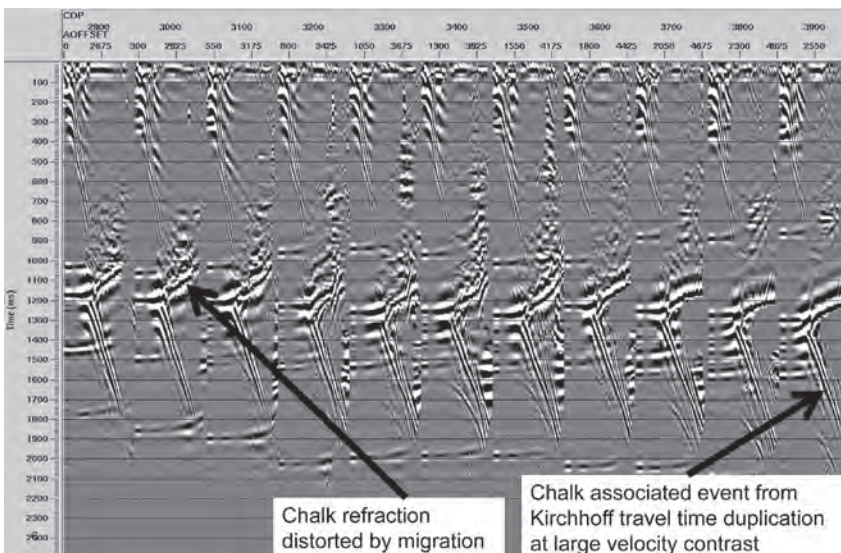


Figure 6 CRP gathers from the preSDM, using the correct velocity model, as shown in Figure 2, converted to time. As with the NMO corrected data, the refracted energy looks anomalous because migration is not designed to handle refracted events. The travel-time duplication events are discussed later, with reference to Figure 9.

In the following figures, most of the modelled data were created using GXT's proprietary 2D modelling code, GXII. This is advantageous because it has options to perform acoustic or elastic, isotropic or anisotropic, modelling using either finite differencing or ray-tracing.

Before considering a 1D multi-layered model (Model 2), let us first consider the behaviour of a half-space model having two solid regions, with a reflecting boundary at some depth between them, and no overlying water layer (Model 3). The results shown in Figure 8 were modelled acoustically using P-wave velocities of 2700 m s⁻¹ and 4800 m s⁻¹, respectively, for the upper and lower layers. These values are representative of the observed real velocities at the top Chalk near well A. In Figure 8a, we see the linear direct wave in the upper solid medium, and the hyperbolic reflection from the half-space boundary with its associated refraction branch beyond the critical angle. Applying NMO with the 1D velocity function including the sharp boundary between 2700 m s⁻¹ and 4800 m s⁻¹ flattens the hyperbolic event, even though the post-critical phase change gives it the appearance of not being very flat, but also introduces the spurious travel-time bifurcation effect (Figure 8b). However, if we apply NMO with a constant velocity of 2700 m s⁻¹, the travel-time bifurcation effect disappears (Figure 8c). In both these figures, the refraction branch curls upwards. Repeating this exercise with a more complex 1D function (Model 2) and applying NMO with this 1D function gives the much more complex, and realistic, behaviour shown in Figure 8d.

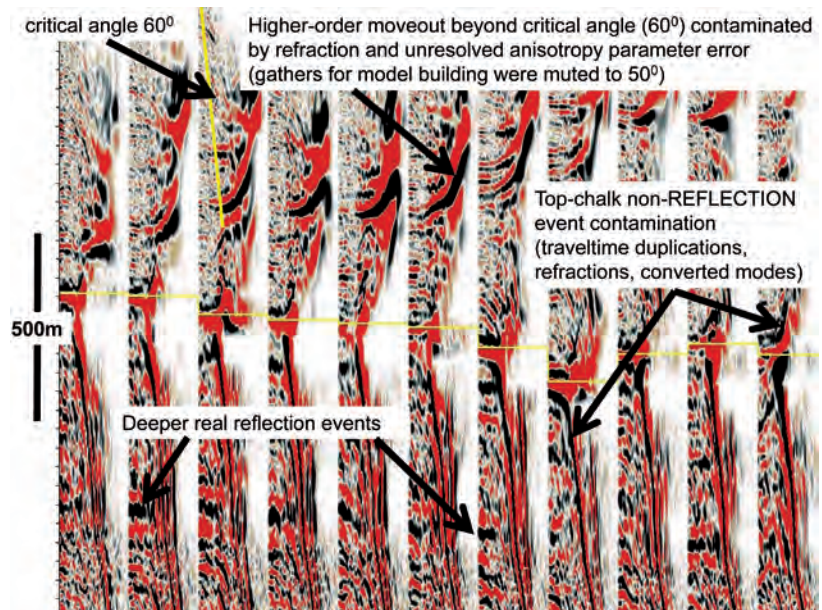
To understand the nature of the NMO travel-time bifurcation, consider the moveout trajectories and migration ray paths shown in Figure 9. For large velocity contrast reflectors, such as the top Chalk, both NMO and Kirchhoff migration can create non-physical events (e.g., Stolk and Symes, 2002, 2004) which have the same travel times as real reflection events (e.g., Aki and Richards, 1980, p. 649; Xu and Huang, 2007).

In Figure 9a, at offset x_1 , a wavelet on the real hyperbolic trajectory emanating from t_1 (blue curve) is moveout-corrected from time t_{in} back to time t_1 . However, also consider the red, higher velocity, curve emanating from t_2 which also passes through the same time, t_{in} , at offset x_1 . NMO repositions a version of the input wavelet to time t_2 as well as to time t_1 . For more benign mild vertical velocity gradients, the wavelet only appears to be stretched as a function of increasing offset, but for a very rapid velocity increase, the wavelet separates out into a distinct event with a characteristic, almost linear trajectory.

In Figure 9b, for source S and receiver R at offset x_1 , the reflection travel path SpR has the same travel time as the non-physical path SabcR, which involves the deeper higher velocity medium. Hence the input wavelet can be 'legitimately' migrated to the associated output location, b, during migration, as well as to the real reflection location, p. Xu and Huang (2007) have proposed picking and using these events as an additional constraint on the tomography. As with the NMO artefact, this spurious event tends to be almost linear.

I now return to consider the multi-layered 1D model. To appreciate the complexity of P-wave reflection processing of non-reflection energy, consider the following individually ray-traced events: water bottom, refraction (diving rays), mid-Tertiary post-critical, and top-Chalk post-critical events (but not yet including the converted modes, to keep things simple). Figure 10a indicates the raypaths for diving rays in the presence of strong vertical compaction velocity gradients. Figure 10b shows the arrivals in a CMP gather for these raypaths. Applying NMO to these and some other events, we can appreciate from Figure 11 that we have a plethora of strange distorted events: these are displayed after NMO on CMP gathers, but the same behaviour is similarly manifested in migrated data.

Figure 7 Real CRP gathers from near the stacked preSDM seismic section shown in Figure 2. Many of the features seen in the modelled data are also present here. Maximum offset is 5.2 km.



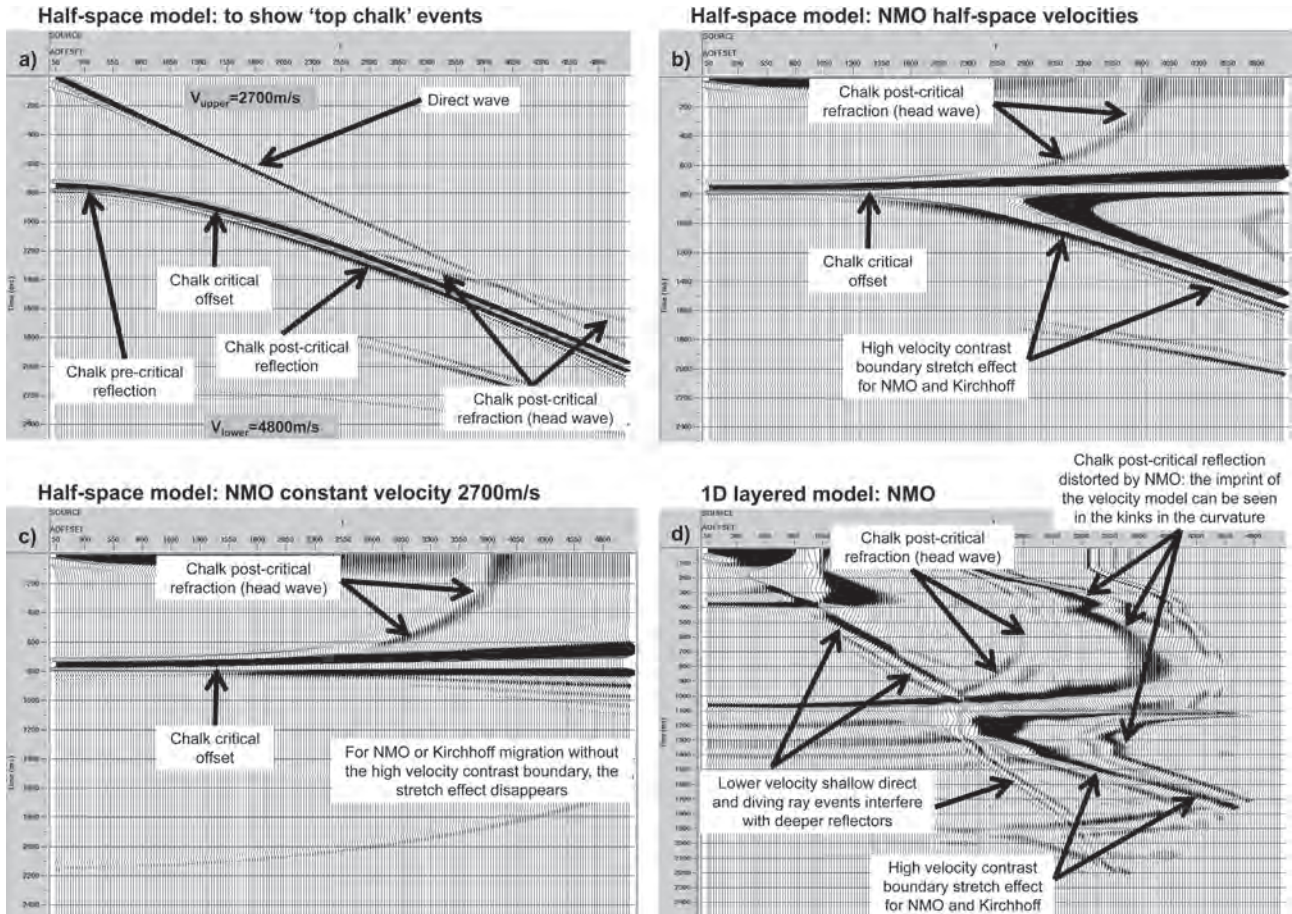


Figure 8 FD acoustic modelling. (a) Reflection and refraction events for a top Chalk reflector model (Model 3). Beyond the critical angle, the phase of the reflection changes. (b) Following NMO with the correct RMS velocity. (c) Following NMO with the velocity of the upper medium, (2700 m s^{-1}). (d) Similar to (b) but for a more complex multi-layered 1D model including a water layer (Model 2). NMO is performed with the more complex 1D RMS function. Again, the downward trending NMO artefact is visible.

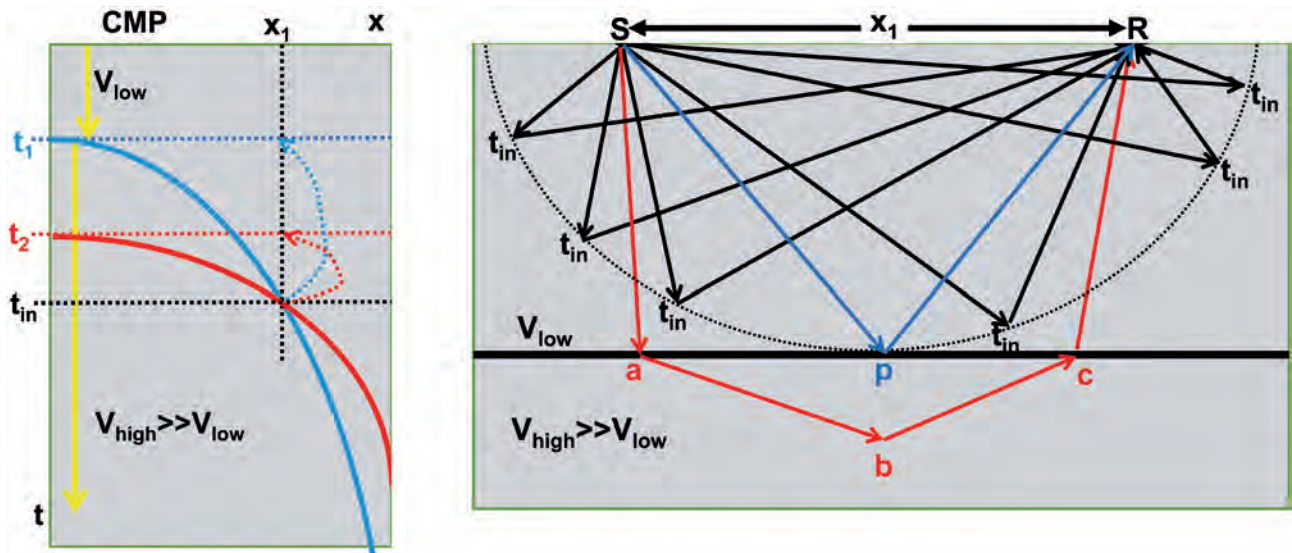


Figure 9 Stretch effect due to high velocity contrast at a boundary for (a) NMO correction, and (b) Kirchhoff migration.

Mode-converted arrivals

For the synthetic modelling performed, mode conversion is associated with the mid-Tertiary and top Chalk reflectors;

but for the purposes of demonstration, I discuss only those related to the top Chalk event because this horizon is present across the entire region. For the various mode-converted

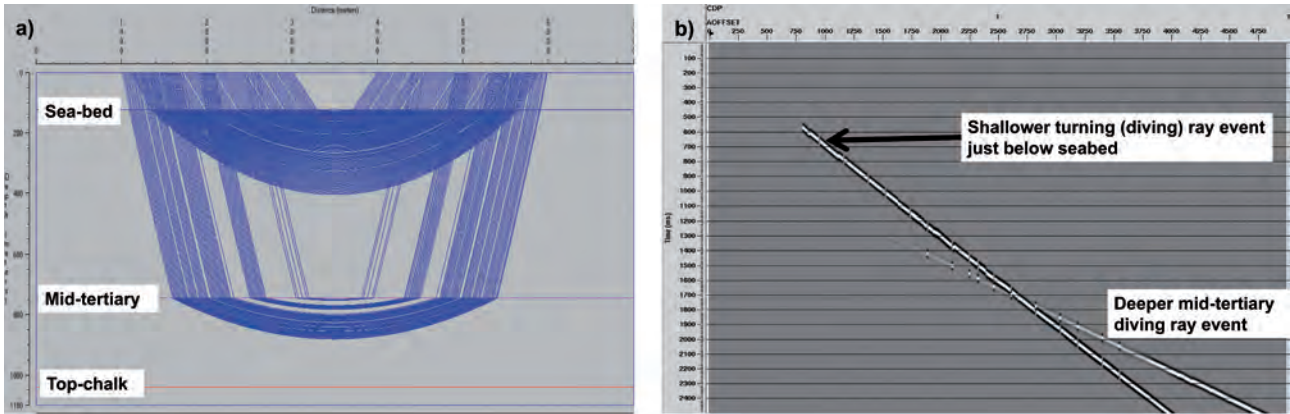


Figure 10 Raypaths for diving rays in the Tertiary and deeper layer. These only exist if there are vertical velocity gradients (e.g., Kaufman, 1953). (b) CMP arrivals for these raypaths.

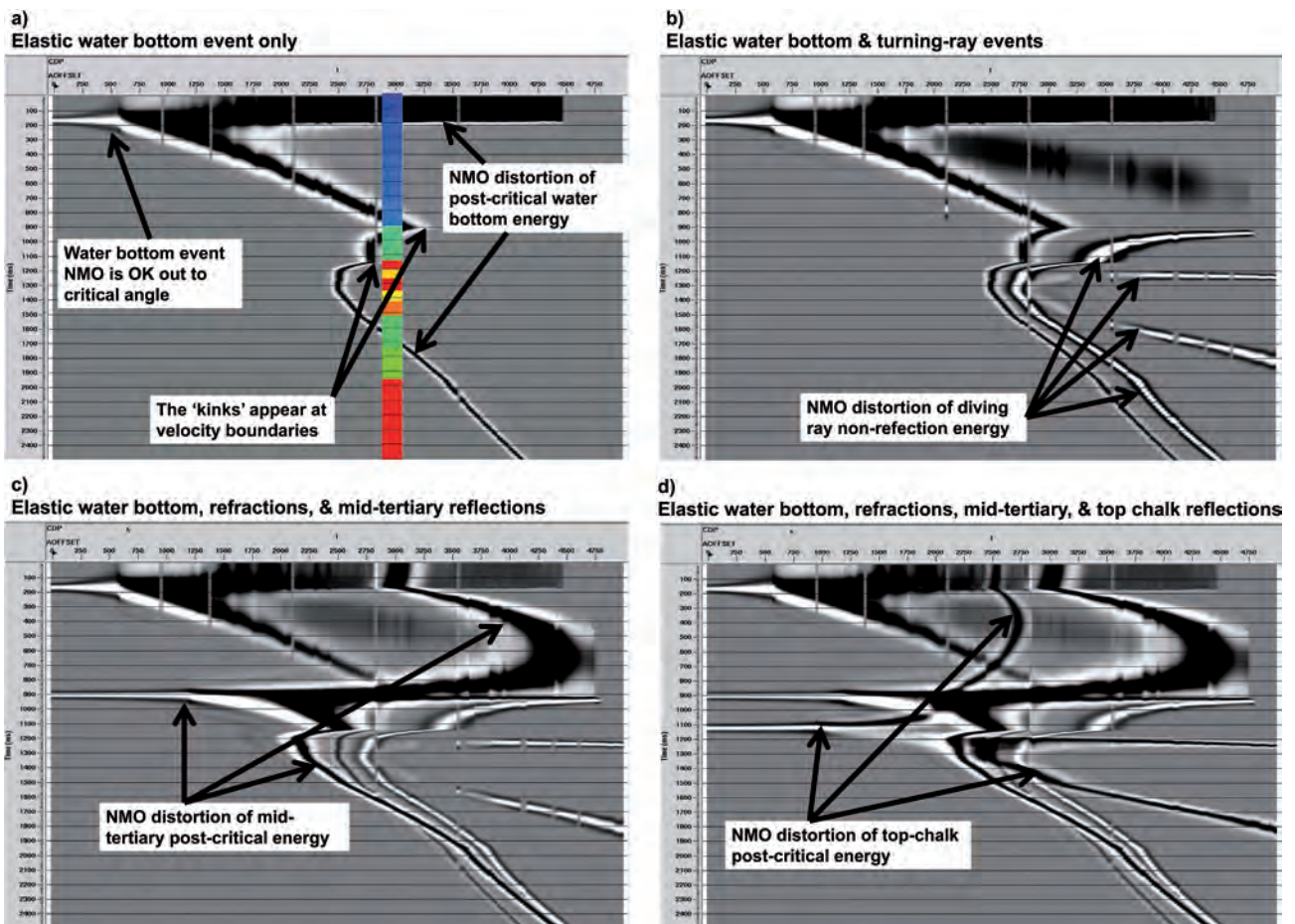


Figure 11 Results of ray-trace modelling to produce various events that show anomalous behaviour in either NMO-corrected or migrated gathers. Events have been added successively to build up a complete picture. Beyond the critical angle, there are both reflected and refracted arrivals. (a) The stretch effect for the water bottom reflection, being distorted by the NMO correction (cf. Figure 9a). The vertical colour bar is included just to indicate the boundary locations in the velocity model. (b) Distortion by NMO of the two linear diving ray events shown in Figure 10. (c) Inclusion of the mid-Tertiary reflection event further complicates the picture, as does (d) inclusion of the top Chalk reflector.

events seen, the conversion takes place at the seabed for transmitted events and at the interfaces where there are high velocity contrasts for reflected events.

Figure 12 shows the elastic ray-trace modelled data for the 1D model (Model 2, Figure 3), with the CMP gather

before and after NMO correction for the top Chalk reflection and associated mode-converted arrivals. Conversion occurs at the seabed for transmission and at the top Chalk for reflection, so we see PSPP, PSSP, and PPSP arrivals, as well as the usual PPPP arrival. The PSPP and PPSP events

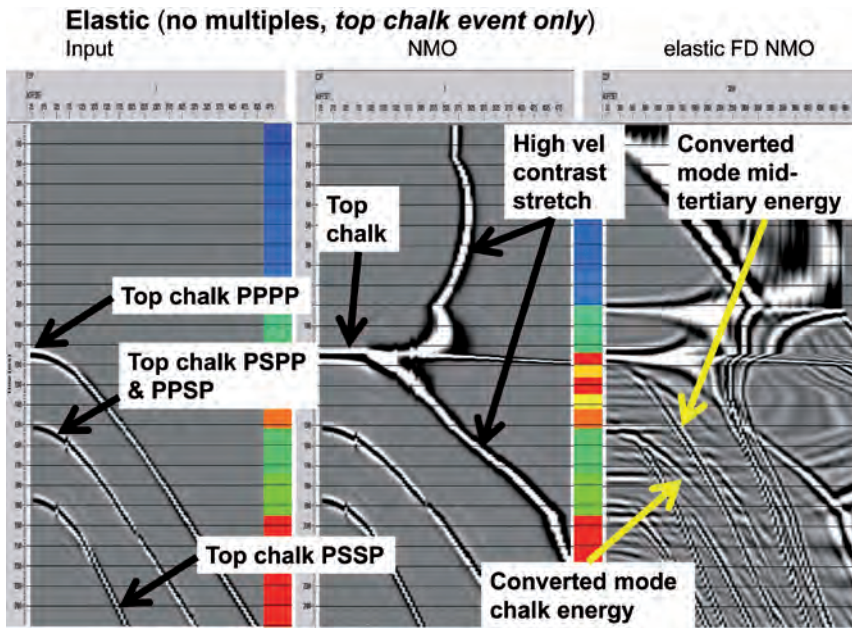


Figure 12 Elastic ray-trace modelled data with 18 Hz peak frequency for the 1D model shown in Figure 3. Left and centre: input CMP gather and CMP gather with NMO correction for the top Chalk reflection and associated mode-converted arrivals. Right: the FD elastic result for comparison, with mode-converted energy from both the Tertiary and top Chalk reflectors and the strong travel-time bifurcation event explained with reference to Figure 9a.

are coincident as their arrival times are the same for the 1D model. On the right is shown the full FD elastic-modelled result for all events in the 1D model, for comparison. In the full FD modelling, there is mode-converted energy from both the Tertiary and top Chalk events. Amplitudes differ between the ray-traced and FD modelled data as ray tracing primarily delivers reasonable kinematics, whereas FD modelling should also produce reasonable dynamics.

Alternative S velocity model

It is unlikely that the mode-converted energy is really so strong on the real data. Up to this point, I have used a Poisson's ratio of 0.25 for all sediments, but I reproduced the work for other models including one with a thin near-seabed layer with very low S-wave velocity ($V_s = 600 \text{ m s}^{-1}$, $V_p = 1600 \text{ m s}^{-1}$, Poisson's ratio = 0.45), and also one with sediments with a Poisson's ratio of 0.33. This reduces, but does not remove, the mode-converted contributions; hence the general conclusions for converted energy still hold. These examples are not included here because they appear very similar. Mode-converted amplitudes on real data could also be reduced by low Q values and extensive near-seabed heterogeneity. It is also worth noting that exceptionally low values of V_s near the seabed have been reported, e.g., $V_s < 50 \text{ m s}^{-1}$ (Jacques Leveille, pers. com.).

Zoeppritz modelling for energy partitioning at interfaces

To assess the likely contribution of mode-converted waves (e.g., Tatham and McCormack, 1991; Pelissier et al., 2007), we can use a Zoeppritz modeller to estimate reflection and transmission energy at each interface, for either upcoming or downgoing waves, for the various propagation models. Here I have used the applet provided to sponsors of the University

of Calgary CREWES consortium. On the basis of the modelling performed, it appears that observable mode-converted energy should be present in the data.

Figure 13a indicates the raypaths being considered for the reflection coefficient analysis, and Figure 13b shows the arrivals for the top Chalk event, indicating the phase change for the reflection at the critical angle and the mode-converted PSPP, PPSP, and PSSP arrivals.

Figure 14 shows the reflection and transmission coefficients for the downgoing water-to-sediment travel path and for the conversion of upcoming S to P at the water bottom. This latter conversion is crucial; otherwise the propagating shear-wave energy cannot pass through the water to be received at the hydrophones as P-waves. It is clear that even for modest offsets in shallow water, we have significant mode-converted amplitudes in the recorded data for the velocity model considered in this study.

Acoustic and elastic modelling, with and without surface multiples

I now describe in more detail the various anomalous events, comparing both acoustic and elastic modelling, with and without surface-related multiples, and following through to preSDM of the data. FD modelling inherently reproduced all interbed multiples associated with the velocity and density models, but with incorrect amplitudes if modelled acoustically. Surface-related multiples can be suppressed by using an absorbing surface boundary condition in the FD code. It is often beneficial to produce initial results without the surface multiples, as this makes it easier to identify what event is what. In the same vein, using ray-trace modelling is of further assistance in identifying individual events, because each raypath can be individually modelled (e.g., double bounces, mode conversions), although the amplitude treatment is often less accurate.

Figure 15 shows the input CMP gather, the CMP gather with NMO, and the depth-migrated CRP gathers for acoustic FD modelled data with an absorbing surface boundary condition, hence no mode conversions (acoustic) and no free-surface multiples or ghosts. Figure 16 makes the same comparison for elastically modelled FD data, where we see the mode-converted arrivals present in the gathers, and Figure 17 shows the elastic data with a reflecting surface boundary condition, so free-surface multiples are included. These latter data are more appropriate for comparison with real data prior to multiple suppression.

Comparison with real data

Unfortunately, the very raw data from the project had long since been archived, so for this study I used the data that was conveniently available. The ‘rawest’ data had already had a first pass of linear noise suppression, but still contains enough remnant linear noise to compare meaningfully with

the modelled data. Figure 18 shows a synthetic CMP created with the 1D model (Model 2) and a real CMP gather where the top Chalk event is indicated with the arrow. Whereas the synthetic also has a strong mid-Tertiary event, the real data do not (this mid-Tertiary event is not consistently strong over the entire area). On the NMO-corrected gathers, the steeply dipping refraction and mode-converted events are visible. The real data have more multiples because the synthetic model does not contain all the real interbed reflectors.

The moveout trajectories of the mode-converted events on the synthetic FD data have been picked on the migrated CRP gather as the yellow dotted lines in Figure 19, and then superimposed on the real data in Figure 20. The real data in the left panel of Figure 20 are those used as input to the migration (with linear noise suppression and some demultiple processing). Both after NMO (centre panel) and after preSDM (right panel), the data still show some remnant noise associated with the mode-converted energy.

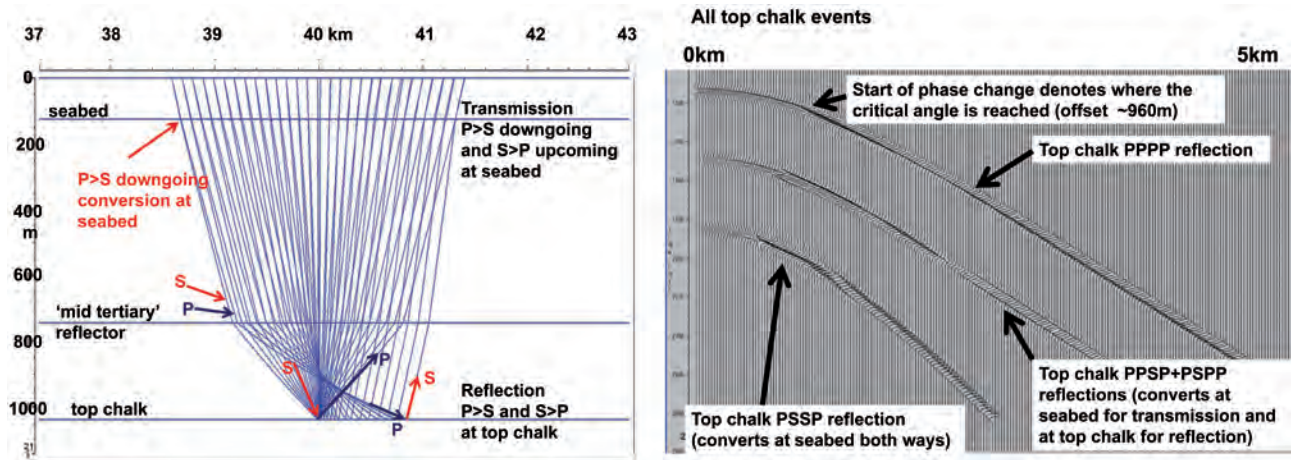


Figure 13 (a) Raypaths associated with mode conversions: at the seabed both the downgoing and upcoming waves undergo mode conversion, and at the mid-Tertiary and top Chalk interfaces, there is also mode conversion on reflection. (b) There is no phase change in the reflected wavelet until the first of the two critical angles. For a large velocity contrast, there is a second critical angle if the S-wave velocity in the lower medium is higher than the P-wave velocity in the upper medium. For the velocity field in the region of this study, post-critical events occur at relatively short offsets.

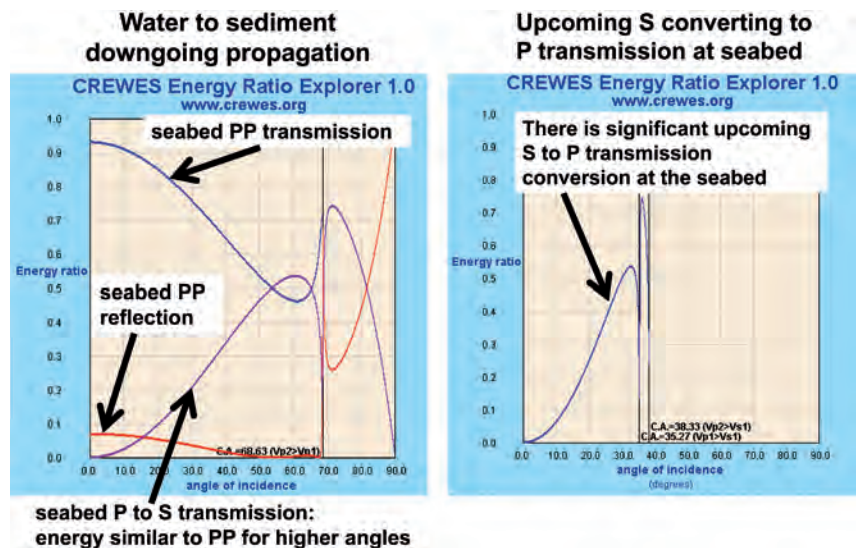


Figure 14 Reflection and transmission coefficients for selected interfaces. Left: at the shallow seabed, the downgoing transmitted P-wave energy has the same magnitude as the S conversion beyond about 40°, which corresponds to an offset of just 220 m for water depth of 80 m. Right: P-wave energy converted to S at the deep reflectors is converted back to P at the seabed. For water, $V_p = 1490 \text{ m s}^{-1}$. For the sediment, $V_p = 1600 \text{ m s}^{-1}$, $V_s = 924 \text{ m s}^{-1}$, Poisson's ratio is 0.25, and density is 1.6 g cm^{-3} .

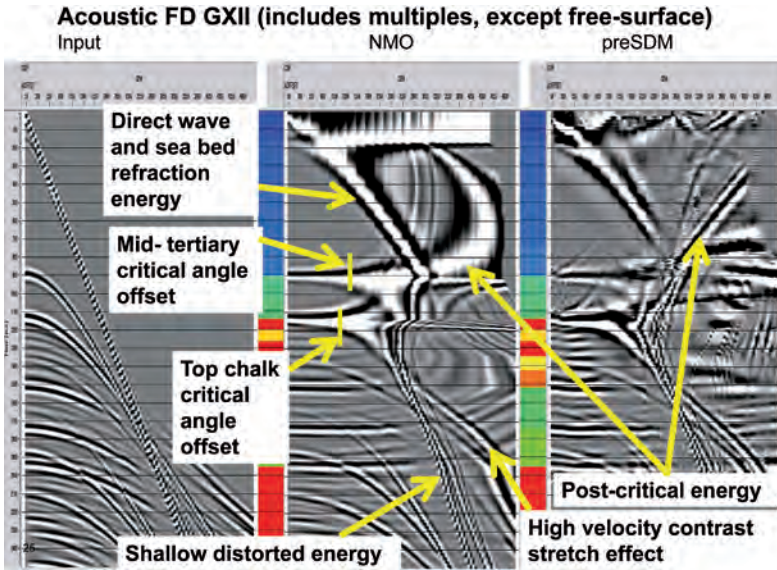


Figure 15 Acoustic FD modelled data for the isotropic 1D model: input CMP gather; CMP gather with NMO correction; and preSDM CRP gather. Free-surface multiples are absent because absorbing boundary conditions were used at the surface.

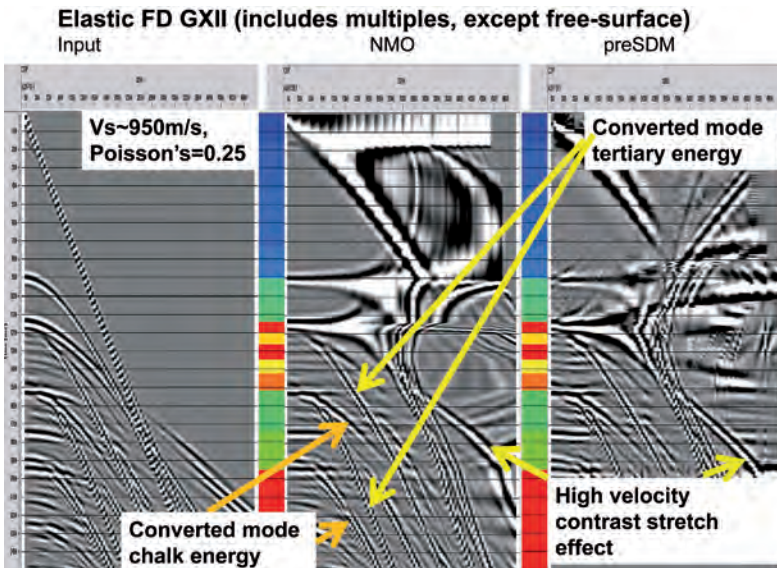


Figure 16 Elastic FD modelled data for the isotropic 1D model: input CMP gather; CMP gather with NMO correction; and preSDM CRP gather. Free-surface multiples are absent because absorbing boundary conditions were used at the surface.

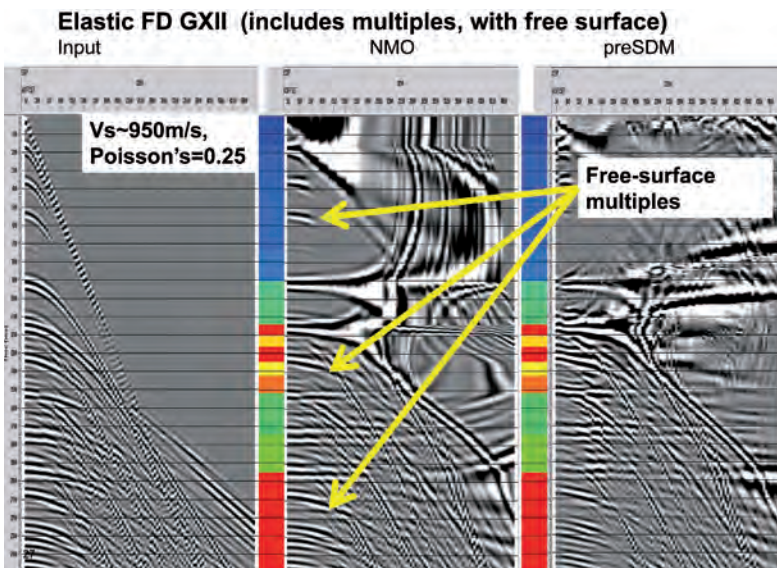


Figure 17 Elastic FD modelled data for the isotropic 1D model: input CMP gather; CMP gather with NMO correction; and preSDM CRP gather. Free-surface multiples are produced by using reflecting boundary conditions at the surface.

Figure 18 Left: FD elastically modelled data with all multiples after NMO correction. Right: real data from an early stage of pre-processing, with a first pass of linear noise removal but no multiple suppression, after NMO correction and bandpass filter to match the modelled data. The families of linear dipping noise below the top Chalk observed on the real data show a close correspondence to the modelled converted and refraction events seen in the synthetic data.

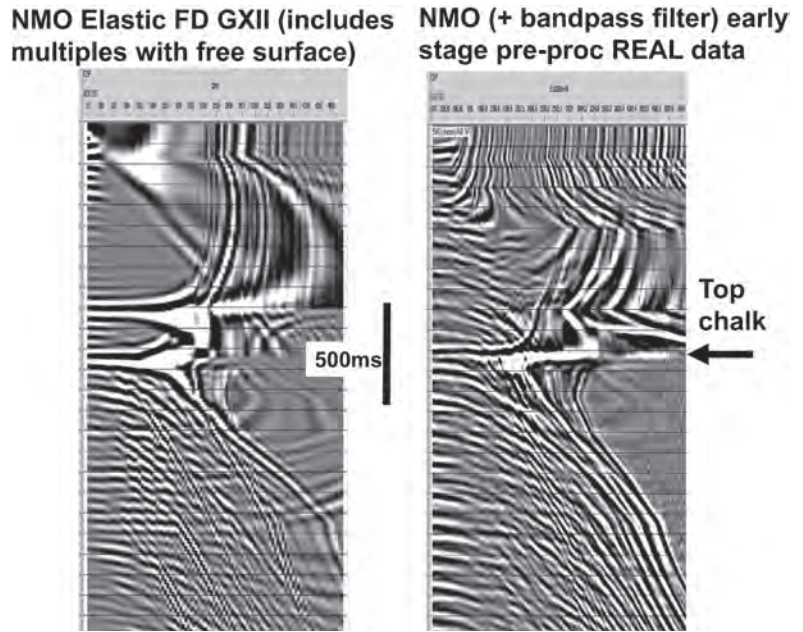
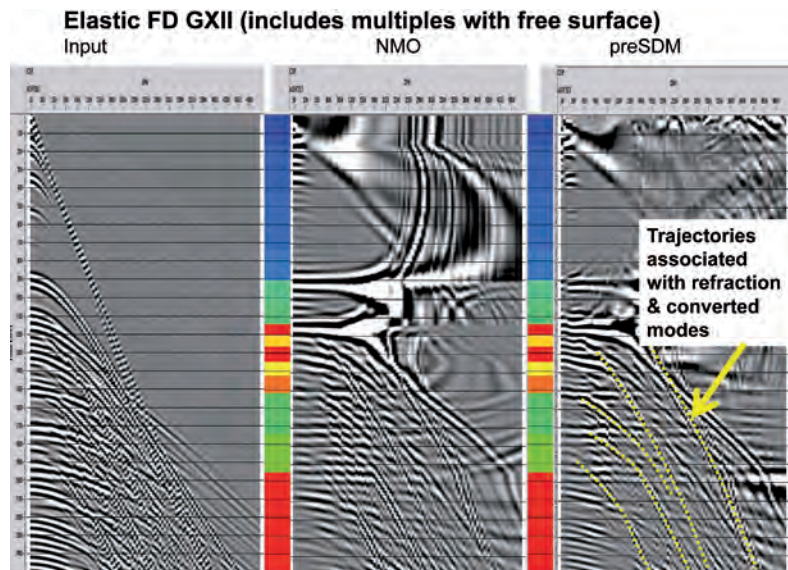


Figure 19 FD elastically modelled data with all multiples: raw data; data after NMO correction; and data after pre-SDM. Superimposed on the migrated gather are manual picks of the moveout trajectories of the converted and refracted events (yellow dotted lines).



The downward (and upward) dipping linear noise from the Chalk refractions can be partly removed using a Radon filter (Figure 21). However, the Radon filter is based on the assumption that moveout trajectories are parabolic, after NMO or migration, whereas the refracted data (both the up-curling and down-curling elements after NMO or migration) are not parabolic. Hence, using an aggressive Radon filter to remove them fully can compromise underlying real events with legitimate residual moveout. Thus, in an iterative velocity model building workflow, use of Radon, and other, filters to remove non-P-reflection energy must be judicious to avoid damaging the underlying reflection residual moveout that we are trying to assess in order to update the velocity model (e.g., Jones, 2010).

Conclusions

Refraction and mode-converted energy is not correctly handled by conventional processing in which it is assumed that each event is a P-wave that has undergone a single reflection. Hence, such energy should ideally be removed prior to migration. However, remnant energy from such events invariably remains in the data after pre-processing, and contaminates the resultant CRP gathers and images. Here I have tried to demonstrate the nature and behaviour of this remnant energy, to give some insight into what details we should be focusing on and what we should be ignoring in resultant gathers and images.

Acknowledgements

I thank Mac Al-Chalabi for a constructive review, Juergen

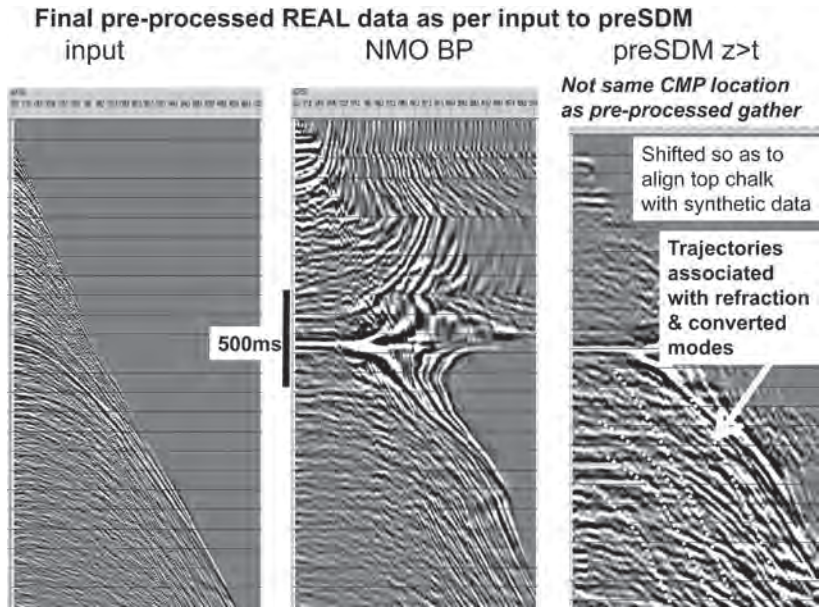


Figure 20 Real data with pre-processing as input to final migration: input data, data after NMO correction; and data after 3D preSDM. The yellow trajectories on the preSDM are the refractions and modelled converted modes from the Tertiary and top Chalk as picked on the migrated gathers of the modelled data. Remnant noise in the real data corresponds with the modelled residual refraction and converted mode events.

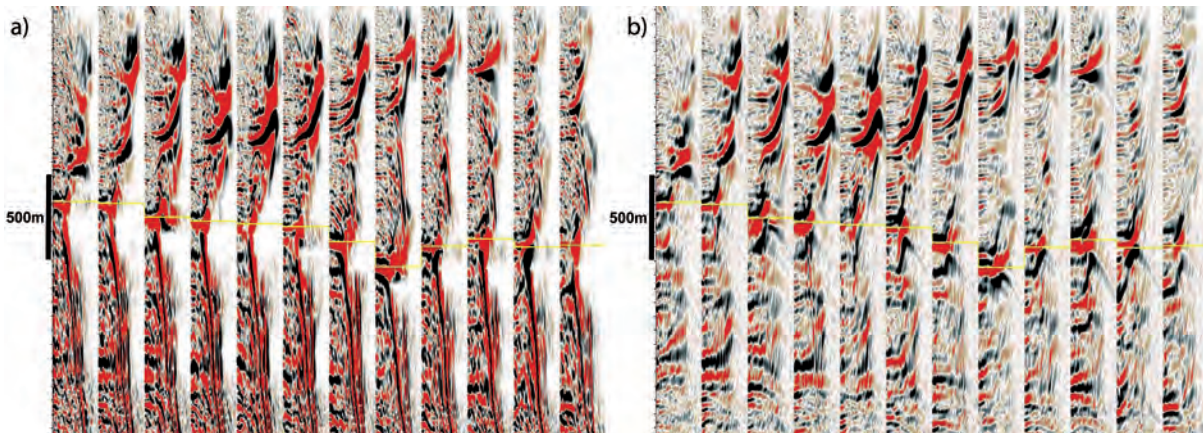


Figure 21 (a) Selection of CRP gathers along a line. There is up-curling noise at shallow levels, resulting from post-critical reflection from the mid-Tertiary reflector, and down-curling noise from the post-critical Chalk reflections. The data were muted to 60° for the autopicking and model update; hence the higher order moveout at shallow levels is not addressed. (b) Same CRP gathers after Radon filter as used in production (dt at 5 km offset is -1000 ms to +3500 ms, with cut at +200 ms). The data input to this process were the migrated gathers shown in Figure 20. The down-curling Chalk-related energy has been removed, but the up-curling shallower noise remains.

Fruehn, Jacques Leveille, and John Brittan for detailed proof reading, and Rob Bloor for insightful discussions on Kirchhoff and NMO behaviour.

References

Aki, K. and Richards, P.G. [1980] *Quantitative Seismology: Theory and Methods*. Freeman, San Francisco.
 Carbone, N.M., Deane, G.B. and Buckingham, M.J. [1998] Estimating the compressional and shear wave speeds of a shallow water seabed from the vertical coherence of ambient noise in the water column. *Journal of the Acoustical Society of America*, 103, 801–813.
 Jones, I.F. [2010] *An Introduction to Velocity Model Building*. EAGE, Houten.
 Kaufman, H. [1953] Velocity functions in seismic prospecting. *Geophysics*, 18, 289–297.
 Muyzert, E. [2006] Seabed properties derived from ambient noise. 68th EAGE Conference & Exhibition, Extended Abstracts, B048.

Pelissier, M.A., Hoerber, H., van de Coevering, N. and Jones, I.F. [2007] *Classics of Elastic Wave Theory*. SEG, Tulsa.
 Shillington, D.P., Minshull, T.A., Peirce, C. and O’Sullivan, J.M. [2008] P and S wave velocities of consolidated sediments from a seafloor seismic survey in the North Celtic Sea Basin, offshore Ireland. *Geophysical Prospecting*, 56, 197–211.
 Stolk, C.C. and Symes, W.W. [2002] Artifacts in Kirchhoff common image gathers. 72nd SEG Annual Meeting, Expanded Abstracts, 1129–1132.
 Stolk, C.C. and Symes, W.W. [2004] Kinematic artifacts in prestack depth migration. *Geophysics*, 69, 562–575.
 Tatham, R.H. and McCormack, M.D. [1991] *Multicomponent Seismology in Petroleum Exploration*. SEG, Tulsa.
 Xu, S. and Huang, T. [2007] Migration artifacts and velocity analysis. 77th SEG Annual Meeting, Expanded Abstracts, 3019–3023.

Received 27 March 2013; accepted 13 April 2013.
 doi: 10.3997/1365-2397.2013018